Sequential transformations in assemblies based on octamolybdate clusters and 1,2-bis(4-pyridyl)ethane†‡

Reinaldo Atencio,*[a] Alexander Briceño,[a] Pedro Silva,[a] José A. Rodríguez[b] and Jonathan C. Hanson[b]

Received (in Montpellier, France) 17th March 2006, Accepted 9th October 2006
First published as an Advance Article on the web 10th November 2006
DOI: 10.1039/b603996k

The new hybrid inorganic–organic solids $[Mo_8O_{26}][H_2bpe]_2$ (**1**), $\{[Mo_8O_{26}(\mu\text{-bpe})][H_2bpe]_2\}_n$ (**2**), $[Mo_8O_{26}(Hbpe)_2][H_2bpe]$ (**3**), and $\{[Mo_8O_{26}][H_2bpe]_2\}_n$ (**4**) were synthesized under hydrothermal conditions. The crystal structure of **1** contains the discrete octamolybdate β-isomer, whereas in **3** the inorganic building unit is a functionalized octamolybdate of general formula $[Mo_8O_{26}X_2]^{(2n+4)}$. A similar building unit is found in **2** and **4**, but forming part of polymeric 1D-arrays. In **2** the polymer is constructed from $[Mo_8O_{26}(\mu\text{-bpe})]^{4-}$, and the functionalization of the anionic cluster in **4** occurs through Mo–O–Mo bonds. The sequential hydrothermal **2**/**3** → **1** and **1** → **4** transformations were observed at 145 and 180 °C, respectively. However, thermal studies of **1** and **4** revealed that both materials do not suffer any phase transitions below 340 °C for **1** or <350 °C for **4**, indicating that such transformations are possible only under the hydrothermal conditions. An XRPD study as a function of the temperature of **1** also demonstrated the negligible structural changes before 330 °C.

Introduction

Polyoxometalates (POMs) and their derivatives represent a unique family of materials that combine chemical and structural diversity with the consequent possibility of modifying their physicochemical properties extensively.[1,2] In the past years, the structural chemistry of these materials has experienced an important growth, assisted by the implementation of new synthetic routes.[3] One of the strategies involves reactions under hydrothermal conditions in which the cooperative assembly between POMs and organic species is allowed to yield attractive hybrid organic–inorganic materials.[3–5] In these synthetic routes, it is possible to modify and/or to functionalize the oxide surfaces of the POMs with a pre-selected organic component.[3–5] Nowadays, some structural tendencies of these materials have been resolved, but only very few studies are known to deal with the mechanisms and/or the intermediate phases responsible for the formation of the final solid during the hydrothermal process.[6–9] Such transformations represent a fundamental aspect to reach a better understanding and potential control of the factors that govern the assembly of hybrid solids. In this report and in order to gain more insight about these transformations, the utilization of the structurally flexible organic component [1,2-bis(4-pyridyl)ethane, (bpe)] was combined with the study of intrinsic variables of the hydrothermal methods (stoichiometry, time and temperature) during the synthesis and structural characterization of the four novel hybrid molybdenum oxide assemblies $[Mo_8O_{26}][H_2bpe]_2$ (**1**), $\{[Mo_8O_{26}(\mu\text{-bpe})][H_2bpe]_2\}_n$ (**2**), $[Mo_8O_{26}(Hbpe)_2][H_2bpe]$ (**3**), and $\{[Mo_8O_{26}][H_2bpe]_2\}_n$ (**4**). It is also shown that these phases are involved in a sequential transformation process under the hydrothermal conditions.

Results and discussion

Overview

Crystals of **1** were obtained as a highly pure single-phase by heating a 1 : 1 molar ratio mixture of heptamolybdate and bpe at 145 °C over two days. Its crystal structure purity was demonstrated from comparison of the diffraction pattern modelled from the single-crystal data and that measured from the bulk (see supplementary material‡). However, when the reaction was carried out over the same time and temperature but using a heptamolybdate : bpe molar ratio of 1 : 2, a mixture of crystalline phases, **1** and **2**, was clearly identified from XRPD patterns. Additionally, a very small amount (non-detectable from XRPD) of crystals of a third phase (**3**) was easily picked up from the bulk under the optical microscope and its crystal structure was determined from single-crystal X-ray measurements (see below). Only phase **1** was detected by XRPD after heating this mixture over five days. Furthermore, both **1** and the last mixture containing **1–3** were transformed to a highly pure phase when the temperature of the reaction was augmented to 180 °C over three days. This phase was further identified to be **4** by using powder and single-crystal XRD experiments and elemental analysis of the bulk.

[a] *Instituto Venezolano de Investigaciones Científicas, (IVIC), Apartado 21827, Caracas, 1020-A, Venezuela. E-mail: ratencio@ivic.ve; Fax: +58-212-5041350; Tel: +58-212-5041609*
[b] *Chemistry Department, Brookhaven National Laboratory, Upton, NY 11973, USA*

† The HTML version of this article has been enhanced with colour images.

‡ Electronic supplementary information (ESI) available: X-Ray powder diffraction patterns, TGA/DSC analysis. See DOI: 10.1039/b603996k.

Crystal structures

$[Mo_8O_{26}][H_2bpe]_2$ (1). The crystal packing of **1** is built up from the assembly of discrete octamolybdate units and H_2bpe^{2+} as a charge-compensating agent. The anionic cluster corresponds to the well-known β-isomer,[10] which is formed by eight edge-sharing $\{MoO_6\}$ distorted octahedra. The cations form an undulated organic sub-network sustained by π–π interactions [average distance: 3.64(3) Å] between the pyridine rings (Fig. 1a). This sub-array allows a set of 3D-cavities where β-$(Mo_8O_{26})^{4-}$ units remain encapsulated (Fig. 1b). The cation–anion interactions occur *via* charge-assisted N^+–H···O hydrogen bonds involving terminal oxo-ligands [N1···O22 = 2.74(2) Å and N2···O12 = 2.86(2) Å]. The final framework architecture suggests that the cations act as an organic scaffolding of the inorganic constituent. Similar examples have been reported previously.[11,12] This feature may be comparable with the scaffolding role that some metal–ligand polymers play in polymolybdate species.[3c]

$\{[Mo_8O_{26}(\mu\text{-bpe})][H_2bpe]_2\}_n$ (2). The crystal packing consists of an unprecedented one-dimensional hybrid coordination polymer $[Mo_8O_{26}(\mu\text{-bpe})]_n^{4n-}$ built up from centrosymmetrical $(Mo_8O_{26})^{4-}$ units linked by bridging bpe molecules which are also located on inversion centres (Fig. 2a). Therefore, the building block of the polymer can be formulated as $[Mo_8O_{26}(\mu\text{-bpe})]^{4-}$, and it is constructed by octahedral moieties. There are six $\{MoO_6\}$ and two $\{MoO_5N\}$ units fused by edge-sharing through bridging oxo-ligands. This octamolybdate maintains a topology which is comparable to that observed for the γ-$(Mo_8O_{26})^{4-}$ isomer.[13] However, this latter γ-isomer displays vacancies in two five-coordinated Mo-centres, whereas in the building block of **2** these vacancies are occupied by N-atoms from two bridging bpe ligands. Therefore, the building unit of **2** represents a class of functionalized octamolybdates that shows the general formula $[Mo_8O_{26}X_2]^{(2n-4)}$,

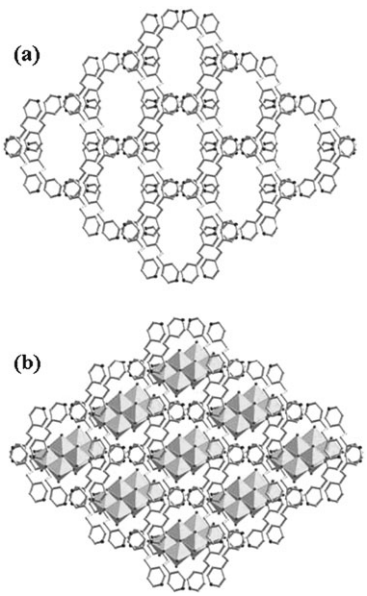

Fig. 1 View of the crystal structure of $[Mo_8O_{26}][H_2bpe]_2$ (**1**) showing the organic sub-network (a) in which β-$(Mo_8O_{26})^{4-}$ units are encapsulated (b).

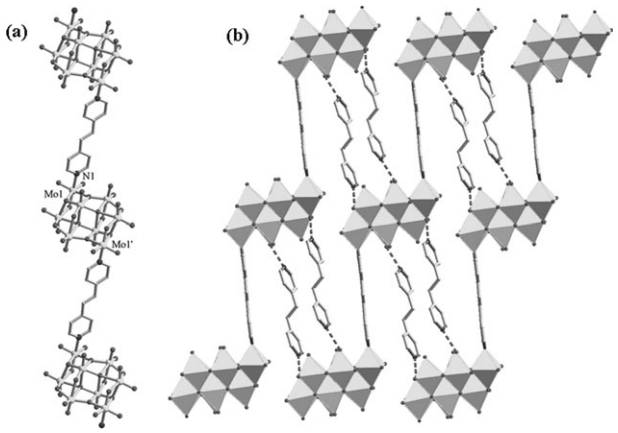

Fig. 2 View of the crystal structure of $\{[Mo_8O_{26}(\mu\text{-bpe})][H_2bpe]_2\}_n$ (**2**) showing (a) the coordination polymer and (b) the parallel arrangement of polymers leaving cavities where H_2bpe^{2+} are hosted.

where *n* is the charge of X.[14] Only a few examples of this anionic moiety have been structurally characterized so far: X = pyridine,[15] imidazole,[16] pyrazole,[17] isothiocyanate[18] and dipyridylamine.[19]

As mentioned before, in this crystal structure a molecule of bpe acts as a spacer, coordinated *via* the nitrogen atoms [Mo1–N1 = 2.264(4) Å]. The polymers display a zig-zag configuration along the [020]-direction (Fig. 2b) and they are accommodated parallel to one another, allowing cavities to host two H_2bpe^{2+} moieties, which are the charge-compensating agents. This 2-D arrangement is stacked parallel to the (101)-plane, assisted by π–π interactions between the organic cations and the bpe spacers [average distance: 3.71(5) Å]. The cations help to sustain the 2D-array by using extra N^+–H···O_t hydrogen bonds, involving terminal oxo-ligands of the clusters [N2···O21 = 2.667(7) Å and N3···O42 = 2.747(7) Å].

$[Mo_8O_{26}(Hbpe)_2][H_2bpe]$ (3). The asymmetric unit of the crystal structure contains a half of one octamolybdate and one $Hbpe^+$ directly N-coordinated to a Mo-centre [Mo1–N1 = 2.269(6) Å]. This centrosymmetrical discrete cluster $[Mo_8O_{26}(Hbpe)_2]^{2-}$ (Fig. 3a) shows similar structure to that of the building block of the coordination polymer in the crystal structure of **2**. In **3**, however, the N-substitution on both $\{MoO_5N\}$ moieties corresponds to that of one monoprotonated terminal $Hbpe^+$ ligand. There exists, therefore, only one double protonated H_2bpe^{2+} entity acting as a charge-compensating agent. The clusters are accommodated in layers, which are stacked along the *a*-direction (Fig. 3b). The self-assembly of the layers occurs *via* interdigitation of the $Hbpe^+$ terminal ligands, which are maintained together by N^+–H···O_t [N2···O21 = 2.73(2) Å] interactions. The terminal organic ligands also interact to retain the clusters in the same layer. Therefore, each uncoordinated pyridine ring forms a π–π interaction [3.96(2) Å] with the coordinated pyridine moiety of a neighbouring cluster (Fig. 3c). The final assembly is assisted by the doubly protonated H_2bpe^{2+} entities located on centrosymmetrical sites just in between the interdigitation

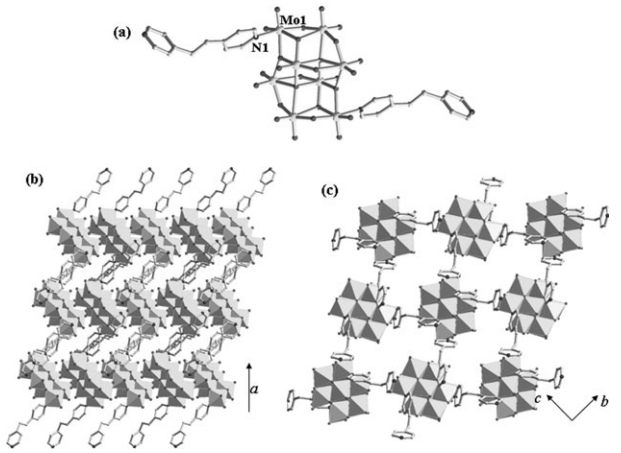

Fig. 3 View of the crystal structure of $[Mo_8O_{26}(Hbpe)_2][H_2bpe]$ (**3**). (a) Molecular structure of the anion $[Mo_8O_{26}(Hbpe)_2]^{2-}$; H-atoms on the terminal ligand $Hbpe^+$ were omitted. (b) Stacking of the layers showing the interdigitation of bipyridine entities in the oxidic interplanar region. (c) View along the *a*-axis of the anionic layer displaying the pyridine rings π–π intermolecular interactions parallel to the *c*-direction.

regions and is also sustained by π–π [3.98(2) Å] and N^+–H···O_t [N3···O41 = 2.83(1) Å] interactions.

$\{[Mo_8O_{26}][H_2bpe]_2\}_n$ (4). The asymmetric unit of the crystal structure contains the same components as those found in **1** (one half of an octamolybdate $Mo_8O_{26}^{4-}$ and one H_2bpe^{2+} unit). However, in **4** the inorganic cluster is assembled through translational repetitions of the corner sharing (Mo1–O22–Mo2^i, $i = 1 - x, -1 - y, 1 - z$) to generate a one-dimensional polymer along the *a*-direction (Fig. 4a). The building block $[Mo_8O_{26}]^{4-}$ of the polymer is constituted from $\{MoO_6\}$ octahedra fused by edge-sharing and its structure corresponds to that of the functionalized γ-octamolybdate, similar to that observed in **2** and **3**. In this case, however, the functionalization is carried out by the formation of two Mo–O–Mo bonds that leads to the polymeric array. The H_2bpe^{2+} units act as counterions, which are located between two parallel polymers and oriented roughly perpendicular to the direction of the polymers. The positions of the cations allow a final 2D-array sustained *via* charge-assisted N^+–H···O hydrogen bonds (Fig. 4b). In contrast to the hydrogen bonding observed in **1**, **2** and **3**, which occurs with terminal oxygen atoms, the N^+–H···O interactions in **4** involve bridging oxygen atoms of the polymer [N1···O24 = 2.833(7) Å; N1···O21 = 2.955(7) Å; N2···O31 = 2.740(6) Å]. This hydrogen bonding facilitates the cations to lie parallel to each other, rendering additional π–π interactions among pyridine rings [average distance: 3.54(1) Å]. The topology of the inorganic polymer observed in **4** is very unusual and has only been reported in the crystal structures of the compounds $\{[H_3N(CH_2)_6NH_3]_2[Mo_8O_{26}]\}_n$[20] and $\{[(Me–NC_5H_5)]_4[Mo_8O_{26}]\}_n$.[21]

As a general features of all crystal structures **1–4**, the Mo–O bond distances and O–Mo–O angles lie in the expected ranges [Mo═O_t = 1.687(4)–1.710(4) Å; for μ_2-O: Mo–O = 1.748(4)–2.257(4) Å; μ_3-O: Mo–O = 1.976(4)–2.379(4) Å; μ_4-O: Mo–O = 1.968(3)–2.477(4) Å; bond angles 71.2(1)–105.8(2)°]. These values are in agreement with those reported in the literature for octamolybdate systems.[22] All the entities, bpe, $Hbpe^+$ and H_2bpe^{2+}, display an *anti* conformation, but show a wide range of dihedral angles between pyridine rings [2.72(5)–99.40(4)°]. Additionally, C–H···O interactions are also observed [range = 2.947(8)–3.277(8) Å], which contribute to stabilize the different frameworks.

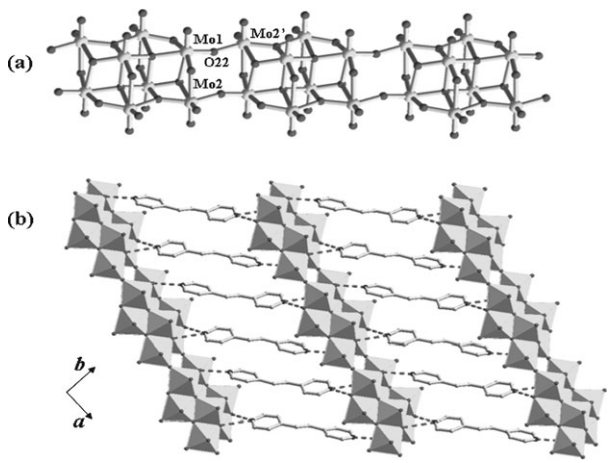

Fig. 4 View of the crystal structure of $\{[Mo_8O_{26}][H_2bpe]_2\}_n$ (**4**). (a) Ball and stick model of the anionic polymer. (b) These polymers are linked together by cations *via* N^+–H···O interactions, allowing a parallel orientation of the oxidic polymers.

Phase transformations under hydrothermal conditions

The presence of the phases **1**, **2** and **3**, observed when the reaction was carried out at 145 °C and using a heptamolybdate : bpe molar ratio of 1 : 2, prompted us to evaluate the influence of the reaction time. A set of reactions was prepared, varying the time of reaction between 1, 2, 3, 4, and 6 days. After heating, the reactors were allowed to cool slowly to room temperature and XRPD patterns were recorded from the resulting solids. The diffractograms (Fig. 5) show that the appearance of **1** and **2** occurs during shorter periods (from one to two days). Only a few crystals of **3** were put on view. However, after longer reaction times solely **1** persists. It is also observed that a non-identified phase appears at three days, but it tends to disappear rapidly when the reaction time is

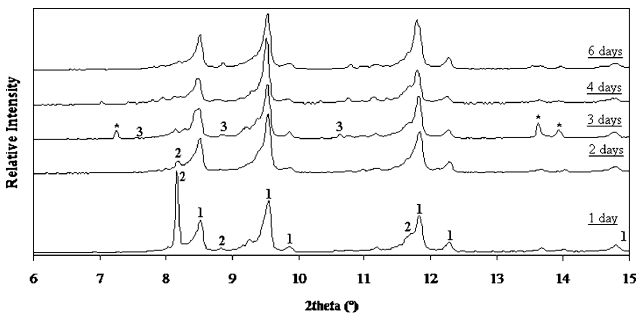

Fig. 5 XRPD patterns of the solids obtained under hydrothermal conditions at 145 °C as a function of the reaction time. Peaks with asterisks correspond to a non-identified phase.

augmented. Additionally, and taking into account the intensity of the peaks in the XRPD patterns, it is noted that at one day the amount of **2** seems to represent an important proportion in comparison to phase **1**. But, this relative presence decreases until phase **2** disappears completely at three days. Intrinsically attached to this observation is the fact that, although the amount of the starting chemicals was always the same, the total weight of each final solid remains comparable (average: 0.114 ± 0.005 g). These results, therefore, suggest that all the phases are involved in transformations between them. In fact, when the mixture of the crystalline phases obtained after one day was used as the starting material and the reaction was carried out over five days, the diffractogram of the resulting solid corresponds to that of the pattern of **1**. It is very interesting to note that such transformations appear to be reached more rapidly when the temperature is increased to 160 °C, in which both phases **2**/**3** are hardly detected in the XRPD patterns from the solid obtained after two days (see supplementary material‡). This behaviour points towards the possibility that at least the formation of **1** and **2** is conditioned by thermodynamic and kinetic control, respectively.

From the crystal structures of **1–3** it is possible to offer some insights about the transformations observed from **2** or **3** to **1** (**2**/**3** → **1**). They would imply (a) one γ → β isomerization of octamolybdate clusters, which is commonly observed in solution and its energetic barrier has been claimed to be very low,[23,24] and (b) the partial or total protonation of the coordinated bipyridine moieties (μ-bpe and $Hbpe^{+}$). It is worth mentioning that the existence of **2** as a polymeric species only occurs in the solid state. In addition, the empirical formulae of **2** and **3** show a different "bpe" : Mo ratio (3 : 8) in comparison to **1** (2 : 8). The last two observations suggest that such **2**/**3** → **1** transformations involve solid–solution disproportionation processes.[25] Such a mechanistic route would go together with the dissociation of the bipyridine moieties due to the relative weakness of the Mo–N bond, which has previously been observed for the analogous cluster functionalized with coordinated pyridine $[Mo_8O_{26}(C_5H_5N)_2]^{4-}$. In this case, the compound is unstable in the presence of water, leading to the loss of pyridine which is accompanied by the formation of the β-Mo_8O_{26} isomer.[15]

On the other hand, the direct **1** → **4** transformation observed at 180 °C involves an augment of the dimensionality from discrete $\{Mo\}_8$ clusters to a 1D-polymer. A plausible explanation could be given in terms of the polymerization of octamolybdate clusters *via* corner sharing (Fig. 6). Supported by the close geometric features observed in both crystal structures (**1** and **4**), it is possible to expect that such a polymerization could occur *via* solid-to-solid topochemical transformation. This process, thus, needs to be accompanied by the low energetic barrier β → γ isomerization. In **1**, for example, the relative orientation of octamolybdate clusters allows intermolecular Mo2···$Mo4^{i}$ ($i = -1.5 - x, -0.5 - y, -z$) distances of 4.42(1) Å, whereas in the polymer of **4** these distances are reduced (Mo1···$Mo2'^{i}$ = 3.72(2) Å ($i = 1 - x, -1 - y, 1 - z$). This possibility was suggested by Zubieta and Rarig[26] in the assembly of the polymeric structure $[CuMo_4O_{13}(H_2bpe)]$ which is built up from γ-octamolybdate

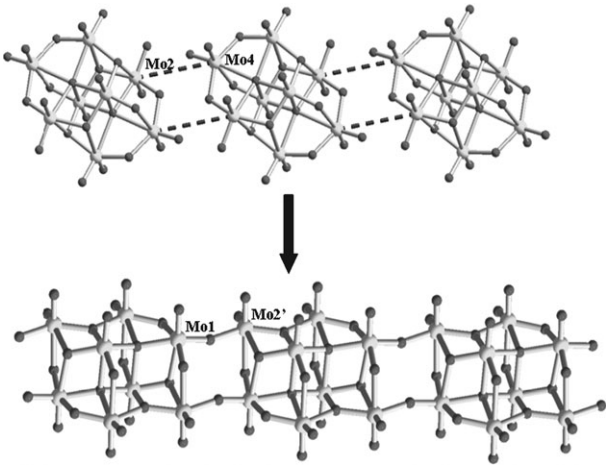

Fig. 6 View of the close geometric features of the inorganic fragments in the crystal structures **1** and **4** [Mo2···Mo4 = 4.42(1) Å for **1**, and Mo1···Mo2′ = 3.72(2) Å for **4**]. A possible route of the **1** → **4** transformation observed at 180 °C.

building blocks. Additionally, similar processes were observed by Müller *et al.* in the spectacular transformations of giant spherical and giant wheel clusters of molybdenum of discrete nature in the solid state at room temperature[27] to produce polymeric arrays in 1- and 2-D. In order to demonstrate this expectation, however, additional information from other techniques concerning *in situ* studies would be required.[6]

Thermal stability analysis of 1 and 4

The thermal studies are consistent with the crystal structures of these compounds. Both TG curves (see supplementary material‡) show a similar behaviour, in which the samples are stable until 350 and 340 °C for **1** and **4**, respectively. A rapid first weight loss step of ~11.7% between 340–380 °C for **1** (~10.7%, 350–400 °C for **4**) is attributed to one released bipyridine molecule (calcd: 11.97%). After that, a continued weight loss occurs until 900 °C (found: ~24.5% for both compounds), which could correspond to sublimation of a Mo_xO_y phase and an intricate decomposition of the second bipyridine along with oxygen atoms of the inorganic oxide released in the form of water molecules (calcd: 14.3%). In both cases, the DSC analysis clearly reveals that two endothermic processes take place below 520 °C under the measurement conditions just associated with the decomposition stage. A striking feature is that these materials do not suffer any phase transitions below 340 °C for **1** (<350 °C for **4**). Therefore, the transformations previously described are possible only under hydrothermal conditions.

In accordance with the thermal analysis, an XRPD study as a function of the temperature of **1** indicates negligible structural changes before 330 °C (see supplementary material‡), except for small displacements from some peak maxima due to the effect induced by the thermal expansion of the crystal packing. After that temperature (>330 °C), the study also shows partial loss of the crystallinity and the appearance of an unknown phase, which further disappears (at ~395 °C) until

the stabilization and growth of the MoO_3 at 480 °C. This latter phase was identified using the powder diffraction files.

Conclusion

In summary, four novel compounds have been successfully isolated and structurally characterized. Starting from the same precursors, but controlling the composition and temperature, it was possible to prepare unprecedented examples of metastable phases. Only compounds **1–3** were observed at temperatures below 160 °C and in short periods of time (1–2 days). However, at 180 °C, such phases correspond to transient phases prior to the formation of a thermodynamically stable compound **4**. These results, together with additional studies carried out by us involving other nitrogen heterocycles,[30] indicate that the formation of metastable phases and the transformation processes are quite concurrent in the synthesis of POMs. Likewise, the compounds **1–4** provide an unusual example of solids that are involved in transformations with preservation of the inorganic building block composition. The rational evaluation of such behaviour, in which a pre-assembled building block is transformed to a related phase, opens a window for the study of the widely recognised intricate mechanisms of formation and/or transformations commonly observed in this important class of solids under hydrothermal conditions.

Experimental

Methods and materials

All reagents were obtained from commercial sources and used without further purification. The syntheses were carried out in 23 mL Teflon-lined autoclaves under autogenous pressure. The elemental analyses were performed (C, H, N) on a model EA1108 Fisons elemental analyzer. The FT-IR spectra were recorded from KBr discs, using a Nicolet Magna-IR 560 spectrophotometer. Thermal analyses (TGA/DSC) were performed in a Dupont 951 thermal analyzer and a Dupont 990 cell, under a dynamic nitrogen atmosphere. For all thermal measurements the heating rate was 10 °C min^{-1} from room temperature until 900 °C (DSC: 530 °C). XRD data were collected in a Siemens D5005 diffractometer with Cu Kα radiation (λ = 1.5418 Å). Time-resolved XRD data were carried out on a MAR diffractometer at the beam line X7B at NSLS, Brookhaven National Laboratory. The wavelength used was 0.9200 Å. Diffraction frames were recorded in 60 s, and the temperature ramp was set from 25 to 480 °C, with a speed of 3 °C min^{-1}.

Syntheses

$[Mo_8O_{26}][H_2bpe]_2$ (1). A mixture of $(NH_4)_6Mo_7O_{24}\cdot 4H_2O$ (Hma; 0.40 mg, 0.33 mmol) and 1,2-bis(4-pyridyl)ethane (bpe; 0.60 mg, 0.33 mmol) in a molar ratio of 1 : 1 in 9 mL of H_2O, was heated at 145 °C for 2 days. After slow cooling to room temperature, pale yellow prism crystals of **1** (77.8 mg) were isolated in a yield of 70% based on Mo. XRD pattern showed that **1** was obtained as pure single-phase (see supplementary material‡). Anal. calcd for $C_{24}H_{28}Mo_8N_4O_{26}$: C, 18.53; H, 1.81; N, 3.60%. Found: C, 18.73; H, 1.76; N, 3.72%. IR (KBr, cm^{-1}): 3600–3200 (br, N^+–H), 1654–1610 and 1485 (s, C=C; s, C=N), 970–900 (s, Mo=O), 850 (s, Mo–O–Mo).

$\{[Mo_8O_{26}(\mu\text{-bpe})][H_2bpe]_2\}_n$ (2) and $[Mo_8O_{26}(Hbpe)_2][H_2bpe]$ (3). Both compounds were obtained from a combination of Hma (0.20 mg, 0.16 mmol) and bpe (0.60 mg, 0.33 mmol) in a molar ratio of 1 : 2 under the same conditions used for **1**. The solid isolated consists of a mixture of crystals of different colours, from which compounds **1**, **2** and **3** were identified by XRD.

$\{[Mo_8O_{26}][H_2bpe]_2\}_n$ (4). Compound **4** can be obtained from direct heating of the components in the same molar ratio used for **1** at 180 °C over 3 days or starting from **1** or from the mixture that contains **1**, **2** and **3**. In all attempts, XRD patterns showed that the resultant solids were obtained as a unique product corresponding to **4** (see supplementary material‡). Anal. calcd $C_{24}H_{28}Mo_8N_4O_{26}$: C, 18.53; H, 1.81; N, 3.60%. Found: C, 19.17; H, 1.47; N, 3.83%. IR (KBr, cm^{-1}): 3600–3300 (br, N^+–H), 1626 and 1506 (m, C=C; m, C=N), 956–900 (s, Mo=O), 850 (s, Mo–O–Mo).

Crystal structure determinations

All intensity data were recorded on a Rigaku AFC-7S diffractometer equipped with a graphite monochromator and Mo Kα radiation (λ = 0.71073 Å) at room temperature. For all crystals three reflections were re-measured every 150 reflections to monitor instrument and crystal stability. Data were corrected for Lp effects and absorption. The first models were solved by direct methods and Fourier techniques. Each refinement was carried out by full-matrix least-squares on $|F|^2$ with anisotropic displacement parameters for non-H atoms. H-atoms on nitrogen were included in their found positions, whereas those on carbon were calculated in ideal positions. Both were refined with isotropic displacement parameters set to 1.2 × U_{eq} of the attached atom. Data reductions were performed using teXsan[28] crystallographic software package, whereas refinement calculations were made using SHELXTL-PLUS.[29]

Crystal data for 1. $C_{24}H_{28}N_4O_{26}Mo_8$, M = 1556.02, monoclinic, a = 16.33(6), b = 11.47(7), c = 21.45(6) Å, β = 103.8(2)°, U = 3902(30) Å^3, T = 298 K, space group $C2/c$, Z = 4, μ(Mo Kα) = 2.584 mm^{-1}, R_{int} = 0.0286, $R1$ = 0.0452 and w$R2$ = 0.1153 for 2809 independent reflections with $I > 2\sigma(I)$.

Crystal data for 2. $C_{18}H_{20}N_3O_{13}Mo_4$, M = 870.13, triclinic, a = 10.716(2), b = 11.128(2), c = 11.666(2) Å, α = 68.08(3), β = 85.50(3), γ = 76.19(3)°, U = 1253.2(4) Å^3, T = 298 K, space group $P\bar{1}$, Z = 2, μ(Mo Kα) = 2.027 mm^{-1}, R_{int} = 0.0296, $R1$ = 0.0351 and w$R2$ = 0.0867 for 3766 independent reflections with $I > 2\sigma(I)$.

Crystal data for 3. $C_{36}H_{40}N_6O_{26}Mo_8$, M = 1740.26, monoclinic, a = 11.581(3), b = 17.146(7), c = 12.875(3) Å, β = 101.45(2)°, U = 2505.7(13) Å^3, T = 298 K, space group $P2_1/c$, Z = 2, μ(Mo Kα) = 2.028 mm^{-1}, R_{int} = 0.1000, $R1$ = 0.0426 and w$R2$ = 0.0880 for 2960 independent reflections with $I > 2\sigma(I)$. The terminal $Hbpe^+$ was found disordered in the

uncoordinated pyridine ring. This disorder was modelled by two sets of positions of the involved atoms.

Crystal data for 4. $C_{12}H_{14}N_2O_{13}Mo_4$, M = 778.01, monoclinic, a = 9.689(2), b = 13.447(3), c = 15.341(2) Å, β = 100.61(1)°, U = 1964.7(7) Å^3, T = 298 K, space group $P2_1/n$, Z = 2, μ(Mo Kα) = 2.567 mm^{-1}, R_{int} = 0.0168, $R1$ = 0.0382 and w$R2$ = 0.0939 for 2821 independent reflections with $I > 2\sigma(I)$.

CCDC reference numbers 272480 (**1**), 272481 (**2**), 272482 (**3**) and 272483 (**4**). For crystallographic data in CIF or other electronic format see DOI: 10.1039/b603996k

Acknowledgements

This work was funded in part by grants from FONACIT (Projects no. LAB-97000821 and G-2005000423).

References

1 (*a*) E. Coronado, C. Giménez-Saiz and C. Gómez-Garcia, *Coord. Chem. Rev.*, 2005, **249**, 1776; (*b*) M. T. Pope, in *Comprehensive Coordination Chemistry II*, ed. A. G. Wedd, Elsevier, Amsterdam, 2004, vol. 4, p. 635; (*c*) C. L. Hill, in *Comprehensive Coordination Chemistry II*, ed. A. G. Wedd, Elsevier, Amsterdam, 2004, vol. 4, p. 679; (*d*) M. T. Pope, *Heteropoly and Isopoly Oxometalates*, Springer-Verlag, Berlin, 1983; (*e*) M. T. Pope and A. Müller, *Angew. Chem., Int. Ed. Engl.*, 1991, **30**, 34; (*f*) M. T. Pope and A. Müller, *Polyoxometalates: from Platonic Solids to Anti-Retroviral Activity*, Kluwer Academic Publishers, Dordrecht, The Netherlands, 1994.

2 C. L. Hill, *Chem. Rev.*, 1998, **98**, 1.

3 (*a*) A. Rabenau, *Angew. Chem., Int. Ed. Engl.*, 1985, **24**, 1026; (*b*) J. W. Johnson, A. J. Jacobson, S. M. Rich and J. F. Brody, *J. Am. Chem. Soc.*, 1981, **103**, 5246; (*c*) P. J. Hagrman, D. Hagrman and J. Zubieta, *Angew. Chem., Int. Ed.*, 1999, **38**, 2638; (*d*) P. J. Hagrman, R. C. Finn and J. Zubieta, *Solid State Sci.*, 2001, **3**, 745.

4 (*a*) P. J. Hagrman, R. L. LaDuca, Jr, H.-J. Koo, R. Rarig, Jr, R. C. Haushalter, M.-H. Whangbo and J. Zubieta, *Inorg. Chem.*, 2000, **39**, 4311; (*b*) P. J. Zapf, R. L. LaDuca, Jr, R. S. Rarig, Jr, K. M. Johnson III and J. Zubieta, *Inorg. Chem.*, 1998, **37**, 3411; (*c*) P. J. Zapf, R. C. Haushalter and J. Zubieta, *Chem. Commun.*, 1997, 321; (*d*) P. J. Zapf, R. C. Haushalter and J. Zubieta, *Chem. Mater.*, 1997, **9**, 2019; (*e*) D. Hagrman, R. P. Hammond, R. Haushalter and J. Zubieta, *Chem. Mater.*, 1998, **10**, 2091.

5 (*a*) S. Chakrabarti and S. Natarajan, *Cryst. Growth Des.*, 2002, **2**, 333; (*b*) C.-P. Cui, J.-C. Dai, W.-X. Du, Z.-Y. Fu, S.-M. Hu, L.-M. Wu and X.-T. Wu, *Polyhedron*, 2002, **21**, 175; (*c*) B. Yan, Y. Xu, N. K. Goh and L. S. Chia, *Chem. Commun.*, 2000, 2169; (*d*) N. Guillou, G. Férey and M. S. Whittingham, *J. Mater. Chem.*, 1998, **8**, 2277; (*e*) L. Xu, C. Qin, X. Wang, Y. Wei and E. Wang, *Inorg. Chem.*, 2003, **42**, 7342.

6 (*a*) A. J. Norquist and D. O'Hare, *J. Am. Chem. Soc.*, 2004, **126**, 6673; (*b*) F. Millange, R. I. Walton, N. Guillou, T. Loiseau, D. O'Hare and G. Férey, *Chem. Mater.*, 2002, **14**, 4448; (*c*) R. I. Walton and D. O'Hare, *Chem. Commun.*, 2000, 2283; (*d*) R. I. Walton, F. Millange, A. Le Bail, T. Loiseau, C. Serre, D. O'Hare and G. Férey, *Chem. Commun.*, 2000, 203; (*e*) R. I. Walton, A. J. Norquist, S. Neeraj, S. Natarajan, C. N. R. Rao and D. O'Hare, *Chem. Commun.*, 2001, 1990; (*f*) F. Millange, R. I. Walton, N. Guillou, T. Loiseau, D. O'Hare and G. Férey, *Chem. Commun.*, 2002, 826; (*g*) T. R. Veltman, A. K. Stover, A. N. Sarjeant, K. M. Ok, P. S. Halasyamani and A. J. Norquist, *Inorg. Chem.*, 2006, **45**, 5529.

7 (*a*) S. Chakrabarti and S. Natarajan, *Angew. Chem., Int. Ed.*, 2002, **41**, 1224; (*b*) C. N. R. Rao, S. Natarajan, A. Choudhury, S. Neeraj and A. A. Ayi, *Acc. Chem. Res.*, 2001, **34**, 80; (*c*) C. N. R. Rao, S. Natarajan, A. Choudhury, S. Neeraj and R. Vaighyanathan, *Acta Crystallogr., Sect. B: Struct. Sci.*, 2001, **B57**, 1.

8 P. M. Forster, A. R. Burbank, C. Livage, G. Férey and A. K. Cheetham, *Chem. Commun.*, 2004, 368.

9 (*a*) A. N. Christensen, A. Bareges, R. B. Nielsen, R. G. Hazell, P. Norby and J. C. Hanson, *J. Chem. Soc., Dalton Trans.*, 2001, 1611; (*b*) D. G. Medvedev, A. Tripathi, A. Clearfield, A. J. Celestian, J. B. Parise and J. Hanson, *Chem. Mater.*, 2004, **16**, 3659.

10 (*a*) C.-D. Wu, C.-Z. Lu, H.-H. Zhuang and J.-S. Huang, *Acta Crystallogr., Sect. E: Struct. Rep. Online*, 2001, **E57**, m349; (*b*) W. T. A. Harrison, *Acta Crystallogr., Sect. C: Cryst. Struct. Commun.*, 1993, **C49**, 1900; (*c*) H.-K. Fun, B.-C. Yip, J.-Y. Niu and X.-Z. You, *Acta Crystallogr., Sect. C: Cryst. Struct. Commun.*, 1996, **C52**, 506; (*d*) Q. Wang, X. Xu and X. Wang, *Acta Crystallogr., Sect. C: Cryst. Struct. Commun.*, 1993, **C49**, 464; (*e*) U. Lee, H.-C. Joo and M. A. Cho, *Acta Crystallogr., Sect. E: Struct. Rep. Online*, 2002, **E58**, m599; (*f*) X. Wang, X.-X. Xu, Q.-Y. Wang and Y.-L. Zhai, *Polyhedron*, 1992, **11**, 1423.

11 D. Hagrman, P. J. Hagrman and J. Zubieta, *Angew. Chem., Int. Ed.*, 1999, **38**, 3165.

12 L. M. Zheng, Y. Wang, X. Wang, J. D. Korp and A. J. Jacobson, *Inorg. Chem.*, 2001, **40**, 1380.

13 M. L. Niven, J. J. Cruywagen and J. B. B. Heyns, *J. Chem. Soc., Dalton Trans.*, 1991, 2007.

14 P. Gouzerh and A. Proust, *Chem. Rev.*, 1998, **98**, 77.

15 E. M. McCarron, J. F. Whitney and D. B. Chase, *Inorg. Chem.*, 1984, **23**, 3275.

16 (*a*) C.-D. Wu, C.-Z. Lu, S. M. Chen, H.-H. Zhuang and J.-S. Huang, *Polyhedron*, 2003, **22**, 3091; (*b*) C.-D. Wu, C.-Z. Lu, W.-B. Yang, S.-F. Lu, H.-H. Zhuang and J.-S. Huang, *J. Cluster Sci.*, 2002, **13**, 55; (*c*) P. Martin-Zarga, J. M. Arrieta, M. C. Muñoz-Roca and P. Gili, *J. Chem. Soc., Dalton Trans.*, 1993, 1551.

17 (*a*) P. Gili, P. A. Lorenzo-Luis, A. Mederos, J. M. Arrieta, G. Germain, A. Castiñeiras and R. Carballo, *Inorg. Chim. Acta*, 1999, **295**, 106; (*b*) P. Gili, P. Martin-Zarga, G. Martin-Reyes, J. M. Arrieta and G. Madariaga, *Polyhedron*, 1992, **11**, 115.

18 B. Kamenar, M. Penavic and B. Marcovic, *Acta Crystallogr., Sect. C: Cryst. Struct. Commun.*, 1988, **C44**, 1521.

19 R. L. LaDuca, Jr, R. S. Rarig, Jr, P. J. Zapf and J. Zubieta, *Inorg. Chim. Acta*, 1999, **292**, 131.

20 Y. Xu, L.-H. An and L.-L. Koh, *Chem. Mater.*, 1996, **8**, 814.

21 B. Modec, J. V. Brenčič and J. Zubieta, *Inorg. Chem. Commun.*, 2003, **6**, 506.

22 F. H. Allen, *Acta Crystallogr., Sect. B: Struct. Sci.*, 2002, **B58**, 380.

23 W. G. Klemperer and W. Shum, *J. Am. Chem. Soc.*, 1976, **98**, 8291.

24 D. G. Allis, R. S. Rarig, E. Burkholder and J. Zubieta, *J. Mol. Struct.*, 2004, **688**, 11.

25 V. V. Samuskevich, O. A. Lukyanchenko and L. N. Samuskevich, *Ind. Eng. Chem. Res.*, 1997, **36**, 4791.

26 R. S. Rarig, Jr and J. Zubieta, *Polyhedron*, 2003, **22**, 177.

27 (*a*) A. Müller, S. K. Das, M. O. Talismanova, H. Bögge, P. Kögerler, M. Schmidtmann, S. S. Talismanov, M. Luban and E. Krickemeyer, *Angew. Chem., Int. Ed.*, 2002, **41**, 579; (*b*) A. Müller, E. Krickemeyer, S. K. Das, P. Kögerler, S. Sabyasachi, H. Bögge, M. Schmidtmann and S. Sarkar, *Angew. Chem., Int. Ed.*, 2000, **39**, 1612; (*c*) A. Müller, S. K. Das, H. Bögge, C. Beugholt and M. Schmidtmann, *Chem. Commun.*, 1999, 1035.

28 *teXsan, Version 1.10*, Molecular Structure Corporation, 9009 New Trails Drive, The Woodlands, TX 77381-5209, USA, 1999.

29 *SHELXTL-PLUS V5.1*, Bruker Analytical X-Ray Systems Inc., Madison, WI, USA, 1999.

30 A. Briceño, PhD Thesis, Centro de Química, Instituto Venezolano de Investigaciones Científicas (IVIC), Venezuela, 2003.

